

**Distorted octahedral coordination of tungstate in a subfamily of specific binding proteins**

Kaspar Hollenstein<sup>†</sup>, Mireia Comellas-Bigler<sup>†</sup>, Loes E. Bevers, Martin C. Feiters, Wolfram Meyer-Klaucke, Peter-Leon Hagedoorn, Kaspar P. Locher

<sup>†</sup> These authors contributed equally to this work.

K. Hollenstein, M. Comellas-Bigler, K.P. Locher (✉)  
Institute of Molecular Biology and Biophysics  
ETH Zurich  
Schafmattstrasse 20  
CH-8093 Zurich, Switzerland  
E-mail: kaspar.locher@mol.biol.ethz.ch  
Fax: +41-44-633-1182

L.E. Bevers, P.L. Hagedoorn  
Department of Biotechnology  
Delft University of Technology  
Julianalaan 67  
2628 BC Delft, The Netherlands

M.C. Feiters  
Department of Organic Chemistry  
Institute for Molecules and Materials  
Faculty of Science  
Radboud University Nijmegen  
Heyendaalseweg 135  
6525 AJ Nijmegen, The Netherlands

W. Meyer-Klaucke  
European Molecular Biology Laboratory  
Hamburg Unit  
Deutsches Elektronen Synchrotron  
Notkestrasse 85  
D-22607 Hamburg, Germany

**Abstract**

Bacteria and archaea import molybdenum (Mo) and tungsten (W) from the environment in the form of the oxyanions molybdate ( $\text{MoO}_4^{2-}$ ) and tungstate ( $\text{WO}_4^{2-}$ ). These substrates are captured by an external, high-affinity binding protein, and delivered to ATP binding cassette (ABC) transporters, which move them across the cell membrane. We have recently reported a crystal structure of the molybdate/tungstate binding protein ModA/WtpA from *Archaeoglobus fulgidus*, which revealed an octahedrally coordinated central metal atom. By contrast, the previously determined structures of three bacterial homologs showed tetracoordinate Mo and W atoms in their binding pockets. Until then, coordination numbers above four had only been found for Mo/W in metalloenzymes where these metal atoms are part of the catalytic cofactors and coordinated by mostly non-oxygen ligands. We now report a high resolution structure of *A. fulgidus* ModA/WtpA, as well as crystal structures of four additional homologs, all bound to tungstate. These crystal structures match X-ray absorption spectroscopy (XAS) measurements from soluble, tungstate-bound protein, and reveal the details of the distorted octahedral coordination. Our results demonstrate that the distorted octahedral geometry is not an exclusive feature of the *A. fulgidus* protein, and suggest distinct binding modes of the binding proteins from archaea and bacteria.

**Keywords:** Tungsten, Binding proteins, Octahedral coordination, Crystal structure, Extended X-ray absorption fine structure

**1 Abbreviations**

2

3 ABC ATP binding cassette

4 ATP Adenosine triphosphate

5 DDT 1,4-Dithio-DL-threitol

6 EDTA Ethylenediaminetetraacetic acid

7 EXAFS Extended X-ray absorption fine structure

8 MES 2-Morpholinoethanesulphonic acid

9 PEG Polyethyleneglycol

10 SAD Single-wavelength anomalous dispersion

11 Tris Tris(hydroxymethyl)aminomethane

12 XAS X-ray absorption spectroscopy

13

## 1 Introduction

2  
3 Molybdenum (Mo) is an essential element throughout biology. Certain archaea and bacteria,  
4 however, are able to use tungsten (W) and some hyperthermophiles even appear to be obligately  
5 dependent on tungsten and incapable of utilizing molybdenum [1, 2]. The two trace metals are  
6 taken up in the form of the oxyanion complexes molybdate ( $\text{MoO}_4^{2-}$ ) and tungstate ( $\text{WO}_4^{2-}$ ). Like  
7 other essential nutrients, these are accumulated from the environment by active transport across  
8 the bacterial or archaeal cell membrane. Uptake is catalyzed by ATP binding cassette (ABC)  
9 transporters that consist of a membrane-integral transport complex, composed of two  
10 transmembrane and two nucleotide-binding domains, and an external substrate binding protein  
11 [3]. The transporter provides a gated passageway across the membrane and powers the  
12 energetically ‘uphill’ translocation through ATP hydrolysis. The specificity is determined by the  
13 binding protein that serves as high-affinity receptor of the substrate with dissociation constants  
14 ( $K_D$ ) in the micromolar, occasionally even in the nanomolar range [4, 5].

15 Significant insight into the structure and function of bacterial and archaeal binding proteins has  
16 been accumulated over the past years. They fall into three classes based on their folds, and all  
17 feature a bi-lobed architecture with a substrate binding site buried between the two halves [4, 5].  
18 We have recently determined the crystal structure of a molybdate/tungstate-binding protein from  
19 the hyperthermophile *Archaeoglobus fulgidus* in its molybdate- and tungstate-bound forms, free  
20 and in complex with the cognate ABC transporter ModBC [6]. Due to the evident similarity of  
21 its fold and sequence to bacterial homologs from *Escherichia coli* and *Azotobacter vinelandii*,  
22 we had termed the protein ModA, and the corresponding transporter ModBC. At present it  
23 remains unknown if *A. fulgidus* accumulates  $\text{MoO}_4^{2-}$ ,  $\text{WO}_4^{2-}$ , or both ions through this Mod  
24 system. Independently, however, it has been proposed that based on biochemical data and  
25 sequence comparisons this transporter family would preferentially facilitate the uptake of  $\text{WO}_4^{2-}$ ,

1 and an alternative name (WtpA) was introduced for the binding protein [7]. In the following, we  
2 will refer to these binding proteins as ModA/WtpA wherever possible.

3 The structure of *A. fulgidus* ModA/WtpA has revealed a binding site for molybdate and tungstate  
4 where the central metal atom is in a hexacoordinate configuration. This octahedral geometry was  
5 rather unexpected and in contrast to the previously solved structures of the two ModA homologs  
6 from *E. coli* and *A. vinelandii*, where the oxygen atoms are tetrahedrally disposed around the  
7 metal center [8, 9]. In line with these two structures the recently published structure of a  
8 homolog from the plant pathogen *Xanthomonas axonopodis* pv. *citri* showed a tetracoordinate  
9 Mo atom in the substrate binding site [10].

10 To determine whether the octahedral geometry was a unique feature of the *A. fulgidus* protein,  
11 and to study the binding mode in more detail, we have determined crystal structures of four  
12 additional archaeal homologs of the ModA/WtpA protein, in addition to a much higher  
13 resolution structure of *A. fulgidus* ModA/WtpA. We find that all five homologs indeed bind  
14 tungstate with an octahedral geometry, and by performing X-ray absorption spectroscopy (XAS)  
15 [11] studies, we demonstrate that this binding mode is also present in solution.

16

## Materials and methods

**Expression and purification of ModA/WtpA proteins.** The relevant genes were amplified by PCR from the genomic DNA of *Archaeoglobus fulgidus* (ATCC 49558D), *Methanosarcina acetivorans* (ATCC 35395), *Methanocaldococcus jannaschii* (ATCC 43067D), *Pyrococcus horikoshii* (ATCC 7860), and *Pyrococcus furiosus* (ATCC 43587). The precise starting and end points of the constructs are indicated in Fig. 1. The resulting fragments were inserted into a modified pET-19b (Novagen), attaching an N-terminal decahistidine affinity tag and a Tobacco Etch Virus (TEV) protease cleavage site. All plasmids were verified by DNA sequencing, which indicated that AfModA was expressed with a nonahistidine tag only.

AfModA, MaModA, MjModA, PhModA, and PfModA (the first two letters indicating the source organism) were over-expressed in the cytoplasm of *Escherichia coli* BL21-CodonPlus(DE3)-RIPL (Stratagene). Cells were grown in Terrific Broth supplemented with 1 % (w/v) glycerol at 37 °C. At an optical density ( $A_{600}$ ) of 0.5-1.0 the temperature was lowered to 25°C and cells were grown into stationary phase where expression was auto-induced. All subsequent purification steps were carried out at room temperature unless stated differently. Cells were harvested by centrifugation and disrupted using a M-110L microfluidizer (Microfluidics) at 15.000 psi external pressure. Insoluble material was removed by centrifugation (40.000 x g for 45 min at 4°C) and the supernatant was loaded onto a NiNTA superflow affinity column (Qiagen). The column was washed with 25 mM and 60 mM imidazole (for AfModA, 80 mM imidazole for all others), and the proteins were eluted with 300 mM imidazole. The buffer was exchanged to 50 mM Tris-HCl pH 8.0, 100 mM NaCl, 0.5 mM EDTA, and 2 mM 1,4-dithio-DL-threitol (DTT) by desalting and the protein was incubated with TEV protease for 16-18 hours at 20°C. The buffer was exchanged to 25 mM Tris-HCl pH 8.0, 250 mM NaCl, and 5 mM imidazole prior to removal of cleavage fragments and uncleaved material by a re-run on a NiNTA superflow column. The proteins were desalted into 5 mM Tris-HCl pH 7.5, 50 mM NaCl

(AfModA, MaModA, MjModA, PfModA) or 10 mM Tris-HCl pH 7.5, 100 mM NaCl (PhModA). For MaModA, MjModA, PfModA, and PhModA, the desalt buffer also contained 1.5 mM Na<sub>2</sub>WO<sub>4</sub>. The proteins were concentrated using Amicon Ultra-15 concentrator units (Millipore) with molecular cutoffs of 10 kDa. Concentrations were 25-30 mg/ml (AfModA), 10-15 mg/ml (MaModA), 10-15 mg/ml (MjModA), 5-10 mg/ml (PhModA), 5-10 mg/ml (PfModA). For AfModA, 1.5 mM Na<sub>2</sub>WO<sub>4</sub> was added to the protein before crystallization.

**Crystallization and structure determination.** AfModA, MaModA, MjModA, PhModA, and PfModA (or WtpA) were crystallized by vapor diffusion in sitting drops at 20 °C against reservoir solutions as follows: AfModA (30 mM Tris-HCl pH 8.4, 160 mM Na<sub>2</sub>SO<sub>4</sub>, 5 % glycerol, 28 % PEG 4000); MaModA (0.5 mM MES-NaOH pH 6.5, 210 mM Mg-acetate, 18 % PEG 8000); MjModA (250 mM NH<sub>4</sub>Cl, 16 % PEG 3350); PhModA (100 mM Bicine-NaOH pH 9.0, 100 mM NaCl, 25 % PEG 600); PfModA (200 mM K-formate, 20 % PEG 3350). The protein to reservoir volume ratio was 1:1. Crystals were cryo-protected as follows prior to flash cooling in liquid nitrogen: AfModA (15 % glycerol); MaModA (30 % glycerol); MjModA (30 % ethylene glycol); PhModA (30 % PEG 600); PfModA (30 % glycerol). Diffraction data was collected at the protein crystallography beamline X06SA at the Swiss Light Source (SLS) and processed using programs from the HKL2000 package [12] or XDS [13]. SAD phases exploiting bound tungstate were used for structure solution throughout, collecting data either at the L<sub>3</sub> absorption edge of tungsten or at a high remote wavelength. The wavelengths used were 0.90018 Å for AfModA, 1.21440 Å for MaModA, 1.2134 Å for PfModA, 1.21420 Å for MjModA, and 1.21475 Å for PhModA. Data statistics are presented in Table 1. Initial phases were obtained using the program SHELXD [14] or CNS [15] and were refined using SHARP [16] in combination with the programs DM [17] and Solomon [18]. Model building was performed using the program O [19]. The atomic model of AfModA was first refined isotropically to convergence using CNS [15] against structure factor amplitudes resulting in  $R_{\text{work}}$  and  $R_{\text{free}}$  of

0.1894 and 0.1986, respectively. Further refinement (using anisotropic B-factors) was carried out against the measured intensities using the program SHELXL [14] in the conjugate gradient (CGLS) mode. All residues were in the most favored or additional allowed regions of the Ramachandran plot except for Ala111 in chain A which exhibited a distinct backbone conformation from the equivalent residue in chain B. Refinement statistics are summarized in Table 1. For the other ModA/WtpA proteins, refinement and automatic water building were performed using CNS [15]. Individual B-factors were refined throughout and all residues were in the most favored or additional allowed regions of the Ramachandran plot, except for one MaModA residue, Ser215, which falls into a generously allowed region.

**XAS measurements.** For the X-ray absorption measurements full-length *A. fulgidus* ModA/WtpA (residues 32-342) was used instead of the C-terminally truncated version used for the crystallographic experiments. Concentrated protein (4.5 mM) in 20 mM Tris-HCl pH 8.0, 150 mM NaCl was incubated with a sub-stoichiometric amount of tungstate (final concentration 3 mM) and compared to 3 mM tungstate ( $\text{Na}_2\text{WO}_4 \cdot 2 \text{H}_2\text{O}$ ) in the same buffer. The  $\text{L}_3$ -edge tungsten X-ray absorption spectra were recorded at beamline D2 of the EMBL Outstation Hamburg at DESY, Germany. The DORIS storage ring operated at 4.5 GeV with the positron beam current ranging from 145 to 80 mA. A Si(111) double-crystal monochromator scanned X-ray energies around the tungsten  $\text{L}_3$ -edge (9.8–11.0 keV). Harmonic rejection was achieved by a focusing mirror (cut-off energy at 20.5 keV) and a monochromator detuning to 50 % of its peak intensity. The sample cells were mounted in a two-stage Displex cryostat and kept at about 20 K. The X-ray absorption spectra were recorded as tungsten  $\text{L}_3$  fluorescence spectra with a Canberra 13-element germanium solid-state detector. While processing a pulse, the detector is frozen (dead time). We ensured that no more than 20 % of the counts occurred in this period and corrected each data point for this effect. For each sample, 15-20 scans were collected and averaged to ensure comparable statistics. X-ray energy calibration was achieved by recording



1 Bragg reflections from a static Si(220) crystal in back-reflection geometry during each scan [20].  
2 Data reduction, such as background removal, normalization, and extraction of the fine structure,  
3 was performed with KEMP [21], assuming a threshold energy  $E_0$  for W of 10.210 eV. Sample  
4 integrity during exposure to synchrotron radiation was checked by monitoring the position and  
5 shape of the absorption edge on sequential scans. No change in redox state or metal environment  
6 was detectable.

7  
8 **Extended X-ray absorption fine structure (EXAFS) analysis.** The extracted tungsten  $L_3$ -edge  
9 (25–800 eV) EXAFS data were converted to photoelectron wave vector  $k$ -space and weighted by  
10  $k^3$ . The spectra were analyzed with EXCURVE [22, 23] version 9.272. The program calculated  
11 the theoretical EXAFS for defined structural models based on the curved wave theory.  
12 Parameters of each structural model, namely the atomic distances ( $R$ ), the Debye-Waller factors  
13 ( $2\sigma^2$ ), and a residual shift of the threshold energy ( $EF$ ), were refined, minimizing the fit index  
14 (FI) [22–24]. An amplitude reduction factor of 1.0 was used throughout the data analysis. For  
15 comparison with the crystallographic coordinates of AfModA, the coordinates of chain A were  
16 read into the EXAFS simulation program with W as the central atom. Before refinement, the W-  
17 O distances that were not expected to be resolved in the EXAFS measurements were lumped  
18 together and averaged: the distances W-O<sub>1</sub>, W-O<sub>2</sub>, and W-O<sub>3</sub> were averaged to 1.71 Å, the  
19 distances W-O <sup>$\epsilon$ 2</sup> (Glu218) and W-O <sup>$\delta$ 1</sup> (Asp153) were averaged to 2.23 Å, while the W-O<sub>4</sub>  
20 distance of 2.00 Å was refined independently. The spatial arrangement of the atoms was taken  
21 from the crystallographic coordinates, and the multiple scattering was calculated on the basis of  
22 3 units, each including the central atom with a pair of *trans* ligands. The number of free  
23 parameters was always inspected to be less than the number of independent data points [25]. The  
24 reduced  $\chi^2$  test was used to verify the significance of an additional ligand contribution [22–24].

## Results

We cloned, expressed, purified and crystallized five homologous ModA/WtpA proteins from the archaea *A. fulgidus* (abbreviated as AfModA), *M. acetivorans* (MaModA), *M. jannaschii* (MjModA), *P. horikoshii* (PhModA), and *P. furiosus* (PfModA). Truncations were applied to these proteins as indicated in Fig. 1. These improved the stability of the proteins in solution and also facilitated better lattice contacts, thus providing better crystals that diffracted to higher resolution. The resolutions of the crystallographic studies were all better than 2 Å, with the lowest being 1.8 Å for the *P. horikoshii* homolog and the highest being 1.07 Å for the *A. fulgidus* protein (Table 1). The fold of the five ModA/WtpA proteins is highly similar to those of the previously studied molybdate-binding proteins ModA from *E. coli* and *A. vinelandii*, and to that of the plant pathogen *X. citri* [8-10]. Comparison of the eight structures reveals only one significant alteration of the fold: the five homologs described in this study contain an additional, four-stranded beta-sheet for which no equivalent is found in the proteins from *E. coli*, *A. vinelandii* and *X. citri* (Fig. 2). However, these inserted secondary structure elements are located on the surface of one of the halves of the protein and, thus, do not affect the architecture of the rest of the molecule nor do they change the arrangement of the oxyanion binding site (Fig. 2a). Whereas all other molybdate- or tungstate-binding proteins described in the literature feature tetrahedral coordination of the metal, the tungsten atoms in the ModA/WtpA proteins described here all have six oxygen ligands in an octahedral coordination. Even though this geometry was observed at lower resolution for the AfModA protein earlier [6], the high resolution and excellent quality of the data allow, for the first time, a precise and detailed description of the unusual tungstate binding site at atomic resolution. Based on the crystallographic data a precision of 0.036 Å for the position of an atom with average B-factor (19.8 Å<sup>2</sup>) can be estimated [26, 27]. However, the positional errors for the atoms in the oxyanion are clearly lower (average B-factor of the tungsten atom and its six oxygen ligands is 9.8 Å<sup>2</sup>), and therefore, the

1 precision of the crystal structure and the EXAFS measurements discussed below are estimated to  
2 be similar.

3 In the *A. fulgidus* ModA/WtpA protein, the coordination sphere of the tungsten atom consists of  
4 three terminal ( $O_{1-3}$ ), one protonated ( $O_4$ ) and two carboxyl oxygens from the protein (Figs. 3  
5 and 4). The carboxyl oxygen ligands are in *cis* disposition and are provided by the side-chains of  
6 Asp153 and Glu218, both located in the same lobe of the protein. These two acidic residues are  
7 replaced by hydrophobic side-chains of either Val or Ala in the binding pockets of the other  
8 ModA proteins (Fig. 2b) and, hence, the central metal atom is bound with a coordination number  
9 of four in the bacterial homologs (Fig. 3b). Inspection of the high-resolution structure of  
10 AfModA reveals that the tungsten atom is offset from the center of the octahedron and displaced  
11 away from the carboxyl oxygens, giving rise to a distorted octahedral geometry. The W-O  
12 distances vary significantly depending on the nature of the ligand and some of the bond angles  
13 differ strongly from the regular octahedron values (Fig. 3a and Table 2). The two W-  
14 O(carboxylate) bonds (2.18-2.24 Å) are much longer than the W-O distances involving terminal  
15 oxygen atoms (1.69-1.74 Å). This is in good agreement with the distance observed between the  
16 carboxyl oxygen of *R*-homocitrate and molybdenum in the FeMo-cofactor of *A. vinelandii*  
17 nitrogenase MoFe-protein and with W/Mo-O(carboxyl) bond lengths determined in the crystal  
18 structures of mandelato, glycolato, and *S*-lactato molybdates and tungstates [28-30]. The short  
19 distances between the metal and the three terminal oxygen atoms are indicative of a partial  
20 double bond character. As discussed by Zhou *et al.* [30] the stronger repulsion between such  
21 oxygen atoms results in increased bond angles between them and, in turn, compressed angles for  
22 bonds involving other atoms (Table 2). The increased length of the W- $O_4$  bond (1.92-2.00 Å) is  
23 probably caused by a postulated proton that we expect to be shared by oxygen  $O_4$  and the second  
24 carboxylate oxygen  $O^{e1}$  of Glu218. This intermediate distance complies well with the length of  
25 the bonds between the tungsten atom and the  $\alpha$ -alkoxyl oxygens in mandelato and *S*-lactato  
26 tungstates and molybdates reported by Zhou *et al.* [29, 30], Cambridge Crystallographic Data

Centre (CCDC) reference codes 227929–227931, 203217–203219, 237819 and 237820. This supports the presence of a shared hydrogen atom that, at the available resolution, cannot be observed in the crystal structure. While the W-O distances involving the three terminal as well as the two carboxyl oxygens match well in the two non-crystallographically related AfModA monomers, the length of the W-O<sub>4</sub> bond does not and appears to be more flexible (Fig. 3a). Furthermore, the octahedral geometry is even more distorted than that of the mandelate complexes which feature two instead of one W-O distance in the 2.0 Å range. Like in the ModA proteins of *E. coli*, *A. vinelandii* and *X. citri* the oxygen ligands O<sub>1-4</sub> are bound to AfModA via several hydrogen bonds. Residues from both lobes of the protein contribute to ligand binding with a total of eight hydrogen bonds (Figs. 3a and 4). The hydrogen donors are the four backbone NH groups of Gly41, Ser42, Ser70, and Cys155 and the four side-chain hydroxyl groups of Ser42, Ser70, Glu218, and Tyr236. In the *E. coli* and *X. citri* homologs only seven such interactions are present with no equivalent for the O<sub>4</sub> to HN-Gly41 hydrogen bond (Fig. 3b). Although the structures of the other four ModA/WtpA homologs were determined at lower resolution, we nevertheless conclude that they have a very similar arrangement of their binding sites with distorted octahedral coordination of the metal centers.

Even though the crystallographic evidence for an octahedral tungsten coordination in ModA/WtpA proteins was convincing, we sought to obtain independent evidence for this geometry by studying the AfModA protein in solution rather than in a crystal lattice. To this end we recorded extended X-ray absorption fine structure (EXAFS) spectra of the tungstate-bound protein and, for comparison, of buffer-dissolved monomeric tungstate (Na<sub>2</sub>WO<sub>4</sub>·2 H<sub>2</sub>O). The EXAFS traces (Fig. 5, upper panel) show interferences between different contributions, which is in part visualized by the peaks in the corresponding Fourier transforms (Fig. 5, lower panel). These are dominated by a peak at 1.7 Å representing the shell of oxygens closely bound to tungsten. For the protein spectrum (trace A), additional contributions at 2.2 and 3.7-4.0 Å are resolved which are absent in the spectrum of dissolved WO<sub>4</sub><sup>2-</sup> (trace B). Both features are

characteristic of the distorted octahedral geometry found in the crystal structures of AfModA and the other four ModA/WtpA homologs. The 2.2 Å shell is evidence for the presence of longer W-O distances in that range. The 3.7-4.0 Å feature is due to the geometry-dependent multiple scattering (4th order) paths W-O<sub>a</sub>-W-O<sub>b</sub>-W, where O<sub>a</sub> and O<sub>b</sub> occupy opposite (*trans*) positions with respect to W. While such contributions are enhanced for O<sub>a</sub>-W-O<sub>b</sub> angles close to 180° as in an octahedral geometry, they are absent in complexes with tetrahedral disposition where all O-W-O angles are 109°. This is the case for monomeric tungstate in buffer (Fig. 5, traces B), which was satisfactorily simulated with four oxygen atoms placed at identical distances from the tungsten center without any assumptions regarding their spatial arrangement. In contrast to the AfModA EXAFS spectra, the previously reported EXAFS spectra of *A. vinelandii* ModA and of three cytoplasmic molybdate-binding proteins all lack the contribution at 2.2 Å as well as the features at 3.7-4.0 Å, indicating tetrahedral coordination geometry in these proteins [31]. Multiple scattering pathways going back and forth through the central atom have been observed before for both biological [32] and non-biological [33] square-planar nickel complexes. In the present case, however, their contribution is very dominant (Fig. S1), in particular in the high-frequency oscillations in the *k*-region 3-5 Å<sup>-1</sup> (Fig. 5, upper panel, trace A). The final simulation (black lines in Fig. 5, traces A) includes W-O contributions of 1.79 (3 O), 2.06 (1 O), and 2.24 Å (2 O). The contribution of the 2.06 Å W-O shell is not resolved in the Fourier transform, yet its inclusion is justified as the quality of the fit to the EXAFS data increases significantly ( $\chi^2$  value drops from  $1.615 \cdot 10^{-6}$  to  $1.0592 \cdot 10^{-6}$ ). Moreover, the position of the feature at 3.7-4.0 Å in the Fourier transform, ascribed to multiple scattering contributions, points to combinations of distances W-O<sub>a</sub> and W-O<sub>b</sub> of 1.8 + 2.2 Å and 1.8 + 2.0 Å, but not 1.8 + 1.8 Å or 2.2 + 2.2 Å. This is in line with the steric disposition of the ligands found in the crystal structure where the two carboxylate oxygens of Asp153 and Glu218 and the protonated oxygen (O<sub>4</sub>) are in facial (*fac*) configuration with the three ligands each occupying coordination sites on the corners of a face of the coordination octahedron (Fig. 3).



## Discussion

The recent discovery of octahedral molybdate and tungstate in the binding site of the periplasmic binding protein ModA/WtpA from the archaeon *A. fulgidus* came as a surprise [6]. Until then, coordination numbers above four had only been found in molybdo- and tungstoenzymes, where the Mo and W atoms are components of the catalytic cofactors and are coordinated by several, mostly non-oxygen ligands [1, 2]. Furthermore, in bacterial extracellular as well as intracellular proteins that bind  $\text{MoO}_4^{2-}$ , molybdenum is bound with a coordination number of four [31]. We solved the structures of five archaeal homologs of the bacterial periplasmic molybdate binding proteins and invariably found hexacoordinate tungsten in their binding pockets. This suggests distinct binding modes of the ModA/WtpA proteins from archaea and bacteria. While the previously determined structures of AfModA with bound tungstate and molybdate unambiguously showed that the two oxyanions were both bound with the same octahedral disposition, the resolution (1.60 Å and 1.55 Å, respectively) [6] was not sufficient for an in-depth analysis of the binding geometry. The 1.07 Å crystal structure presented here allows a detailed description of the distorted octahedral geometry including bond lengths and angles, which agree well with those determined from small molecule crystal structures of hexacoordinate monomeric tungstates and molybdates. In addition, our simulations of the X-ray absorption data based on the coordinates of the previously solved structure of tungstate-bound AfModA (PDB ID 2ONS) only poorly matched the EXAFS spectra (not shown), but drastically improved when the more accurate coordinates from the high-resolution structure became available. This indicates the absence of significant photo-reduction during the X-ray diffraction experiment of the protein crystals.

Enhancement of the coordination number and the associated change in geometry is not a requirement for high-affinity binding, as the bacterial homologs from *E. coli* and *X. citri* exhibit affinities with dissociation constants ( $K_D$ ) in the low micromolar range [34, 35]. Yet, imposing a

1 change in coordination chemistry is an effective way to distinguish molybdate and tungstate  
2 from highly abundant sulfate ( $\text{SO}_4^{2-}$ ), since, under physiological conditions, sulfur is unable to  
3 undergo this transition [36]. From the structures of *A. vinelandii* and *E. coli* ModA, where  
4 molybdate and tungstate have only four oxo ligands, it was concluded that these proteins  
5 discriminate between molybdate/tungstate and sulfate mainly by the sizes of these oxyanions [8,  
6 9].

7 With the presence of two additional oxygen ligands, donated by acidic amino acid side-chains,  
8 the affinity for the substrate drastically increases. For *P. furiosus* ModA/WtpA,  $K_D$  values of 17  
9 pM (tungstate) and 11 nM (molybdate) have recently been reported [7]. However, whether the  
10 rather large difference in affinity for these two oxyanions means that this transport system  
11 preferentially takes up tungstate remains to be elucidated. Furthermore, although high affinity is  
12 essential for effective capturing of substrates of low abundance such as trace metals, efficient  
13 transport may only occur if binding proteins readily release their cargo into the translocation  
14 pathway of their cognate ABC transporters. Further biochemical investigation of the transport  
15 process is needed to clarify this point.

16



**References**

1. Hille R (2002) Trends Biochem Sci 27:360-367
2. Johnson MK, Rees DC, Adams MW (1996) Chem Rev 96:2817-2840
3. Holland IB, Cole SPC, Kuchler K, Higgins CF (eds) (2003) ABC Proteins : From Bacteria to Man. Academic Press, London
4. Quioco FA, Ledvina PS (1996) Mol Microbiol 20:17-25
5. Wilkinson AJ, Verschueren KHG (2003) In: Holland IB, Cole SPC, Kuchler K, Higgins CF (eds) ABC Proteins : From Bacteria to Man. Academic Press, London, pp. 187-207
6. Hollenstein K, Frei DC, Locher KP (2007) Nature 446:213-216
7. Bevers LE, Hagedoorn PL, Krijger GC, Hagen WR (2006) J Bacteriol 188:6498-6505
8. Hu Y, Rech S, Gunsalus RP, Rees DC (1997) Nat Struct Biol 4:703-707
9. Lawson DM, Williams CE, Mitchenall LA, Pau RN (1998) Structure 6:1529-1539
10. Balan A, Santacruz-Perez C, Moutran A, Ferreira LC, Neshich G, Goncalves Barbosa JA (2008) Biochim Biophys Acta 1784:393-399
11. Strange RW, Feiters MC (2008) Curr Opin Struct Biol 18:609-616
12. Otwinowski Z, Minor W, Charles W. Carter, Jr. (1997) Methods Enzymol 276:307-326
13. Kabsch W (1993) J Appl Crystallogr 26:795-800
14. Sheldrick GM (2008) Acta Crystallogr A 64:112-122
15. Brunger AT, Adams PD, Clore GM, DeLano WL, Gros P, Grosse-Kunstleve RW, Jiang JS, Kuszewski J, Nilges M, Pannu NS, Read RJ, Rice LM, Simonson T, Warren GL (1998) Acta Crystallogr D Biol Crystallogr 54:905-921
16. de La Fortelle E, Bricogne G, Charles W. Carter, Jr. (1997) Methods Enzymol 276:472-494
17. Cowtan KD, Main P (1996) Acta Crystallogr D Biol Crystallogr 52:43-48
18. Abrahams JP, Leslie AGW (1996) Acta Crystallogr D Biol Crystallogr 52:30-42
19. Jones TA, Zou JY, Cowan SW, Kjeldgaard M (1991) Acta Crystallogr A 47:110-119

- 1    20. Pettifer RF, Hermes C (1985) *J Appl Crystallogr* 18:404-412
- 2    21. Korbas M, Marsa DF, Meyer-Klaucke W (2006) *Rev Sci Instrum* 77 DOI
- 3        10.1063/1.2209954
- 4    22. Gurman SJ, Binsted N, Ross I (1984) *J Phys C Solid State Phys* 17:143-151
- 5    23. Gurman SJ, Binsted N, Ross I (1986) *J Phys C Solid State Phys* 19:1845-1861
- 6    24. Binsted N, Strange RW, Hasnain SS (1992) *Biochemistry* 31:12117-12125
- 7    25. Stern EA (1993) *Phys Rev B Condens Matter* 48:9825-9827
- 8    26. Cruickshank DW (1999) *Acta Crystallogr D Biol Crystallogr* 55:583-601
- 9    27. Blow DM (2002) *Acta Crystallogr D Biol Crystallogr* 58:792-797
- 10   28. Einsle O, Tezcan FA, Andrade SL, Schmid B, Yoshida M, Howard JB, Rees DC (2002)
- 11        *Science* 297:1696-1700
- 12   29. Zhou ZH, Hou SY, Cao ZX, Wan HL, Ng SW (2004) *J Inorg Biochem* 98:1037-1044
- 13   30. Zhou ZH, Zhao H, Tsai KR (2004) *J Inorg Biochem* 98:1787-1794
- 14   31. Duhme AK, Meyer-Klaucke W, White DJ, Delarbre L, Mitchenall LA, Pau RN (1999) *J*
- 15        *Biol Inorg Chem* 4:588-592
- 16   32. Ha SW, Korbas M, Klepsch M, Meyer-Klaucke W, Meyer O, Svetlitchnyi V (2007) *J Biol*
- 17        *Chem* 282:10639-10646
- 18   33. Metselaar GA, Schwartz E, de Gelder R, Feiters MC, Nikitenko S, Smolentsev G, Yalovega
- 19        GE, Soldatov AV, Cornelissen JJ, Rowan AE, Nolte RJ (2007) *Chemphyschem* 8:1850-
- 20        1856
- 21   34. Rech S, Wolin C, Gunsalus RP (1996) *J Biol Chem* 271:2557-2562
- 22   35. Balan A, Santacruz CP, Moutran A, Ferreira RC, Medrano FJ, Perez CA, Ramos CH,
- 23        Ferreira LC (2006) *Protein Expr Purif* 50:215-222
- 24   36. Fraústo da Silva JJR, Williams RJP (2005) *The biological chemistry of the elements: The*
- 25        *inorganic chemistry of life*. Oxford University Press, Oxford
- 26   37. Bendtsen JD, Nielsen H, von Heijne G, Brunak S (2004) *J Mol Biol* 340:783-795

1 38. Holm L, Park J (2000) Bioinformatics 16:566-567

2

3

4

1 **Acknowledgments.** We thank the beamline staff at the Swiss Light Source (SLS) for assistance  
2 with diffraction data collection, and D. C. Rees for discussions. This work was supported by the  
3 Roche Research Fund, the National Center for Competence in Research (NCCR) Structural  
4 Biology Zurich, the Swiss National Science Foundation, and the European Commission,  
5 Research Infrastructure Action under FP6 “Structuring the European Research Area Specific  
6 Programme”, Contract # RII3-CT-2004-506008 for supporting access to the EMBL.

7  
8 **Coordinates.** The coordinates and structure factors have been deposited in the Protein Data  
9 Bank (PDB) under the PDB IDs 3CIJ (AfModA), 3CFX (MaModA), 3CG1 (PfModA), 3CFZ  
10 (MjModA), and 3CG3 (PhModA).

**Table 1: Diffraction data collection and refinement statistics**

	AfModA <sup>a</sup>	MaModA <sup>a</sup>	PfModA <sup>a</sup>	MjModA <sup>a</sup>	PhModA <sup>a</sup>
<b>Data Collection</b>					
Space group	$P2_12_12_1$	$C2$	$P2_1$	$P2_12_12_1$	$P2_12_12_1$
Molecules per AU	2	2	2	1	1
Cell dimensions					
a, b, c (Å)	73.901	115.500	46.460	36.954	37.880
	75.396	51.860	109.792	59.180	89.589
	116.996	124.048	55.430	150.759	97.868
$\alpha, \beta, \gamma$ (°)	90.000	90.000	90.000	90.000	90.000
	90.000	116.933	96.221	90.000	90.000
	90.000	90.000	90.000	90.000	90.000
Resolution (Å) <sup>b</sup>	30.0-1.07	30.0-1.6	30.0-1.6	30.0-1.7	30.0-1.8
	(1.09-1.07)	(1.7-1.6)	(1.7-1.6)	(1.75-1.7)	(1.85-1.8)
$R_{\text{meas}}$ or $R_{\text{sym}}$ (%) <sup>b</sup>	11.8 (39.1)	4.9 (27.6)	8.7 (19.6)	12.8 (21.6)	15.1 (36.1)
$I/\sigma I$ <sup>b</sup>	16.8 (5.1)	15.3 (5.0)	9.5 (5.8)	15.0 (11.5)	16.3 (7.7)
Completeness (%) <sup>b</sup>	99.8 (99.3)	97.1 (95.3)	96.9 (98.0)	99.5 (98.4)	100.0 (100.0)
Redundancy <sup>b</sup>	9.1 (6.6)	3.3 (3.3)	2.6 (2.7)	11.8 (11.9)	13.5 (13.4)
<b>Refinement</b>					
Refinement program(s) used	CNS, SHELXL-97	CNS	CNS	CNS	CNS
Resolution (Å)	10.0-1.07	30.0-1.6	30.0-1.6	30.0-1.7	30.0-1.8
No. of reflections	270746/14081	156891/8211	126782/13648	64186/4812	54468/4037
$R_{\text{work}}/R_{\text{free}}$ (%)	12.64 <sup>c</sup> /14.93	21.03/23.53	18.63/20.46	18.52/20.04	19.90/22.75
No. of atoms					
Protein	4827	4566	4740	2343	2532
$\text{WO}_4^{2-}$	10	10	10	5	5
Water	824	424	525	316	217
Mean $B$ -factors (Å <sup>2</sup> )					
Protein	17.3	26.0	18.7	11.5	24.3
$\text{WO}_4^{2-}$	9.9	20.1	10.9	12.2	16.2
Water	34.6	37.3	39.7	28.0	35.9
R.m.s deviations					
Bond lengths (Å)	0.007	0.0104	0.0097	0.0119	0.0112
Bond angles (°)	0.021 <sup>d</sup>	1.7	1.7	1.6	1.8

<sup>a</sup> The first two letters of the protein name denote the source organism, see Methods.<sup>b</sup> Highest resolution shell is shown in parenthesis.<sup>c</sup> This  $R$ -factor was calculated including all data and is therefore called  $R$  instead of  $R_{\text{work}}$ .<sup>d</sup> R.m.s. deviation for angle distances in Å calculated by SHELXL-97.

1 **Table 2: Oxyanion geometry in AfModA**

	Chain A (°)	Chain B (°)	Average (°)	$\Delta$ (°)
O <sub>1</sub> –W–O <sub>2</sub>	98.7	103.4	101.1	4.7
O <sub>1</sub> –W–O <sub>3</sub>	100.2	100.3	100.3	0.1
O <sub>1</sub> –W–O <sub>4</sub>	157.6	156.0	156.8	1.6
O <sub>1</sub> –W–O <sup><math>\delta</math>1</sup> Asp <sup>153</sup>	81.5	82.0	81.8	0.5
O <sub>1</sub> –W–O <sup><math>\epsilon</math>2</sup> Glu <sup>218</sup>	85.0	83.9	84.5	1.1
O <sub>2</sub> –W–O <sub>3</sub>	102.3	102.5	102.4	0.2
O <sub>2</sub> –W–O <sub>4</sub>	92.2	90.0	91.1	2.2
O <sub>2</sub> –W–O <sup><math>\delta</math>1</sup> Asp <sup>153</sup>	86.6	84.5	85.6	2.1
O <sub>2</sub> –W–O <sup><math>\epsilon</math>2</sup> Glu <sup>218</sup>	170.4	167.6	169.0	2.8
O <sub>3</sub> –W–O <sub>4</sub>	96.6	96.0	96.3	0.6
O <sub>3</sub> –W–O <sup><math>\delta</math>1</sup> Asp <sup>153</sup>	170.5	171.7	171.1	1.2
O <sub>3</sub> –W–O <sup><math>\epsilon</math>2</sup> Glu <sup>218</sup>	85.6	85.8	85.7	0.2
O <sub>4</sub> –W–O <sup><math>\delta</math>1</sup> Asp <sup>153</sup>	79.7	79.5	79.6	0.2
O <sub>4</sub> –W–O <sup><math>\epsilon</math>2</sup> Glu <sup>218</sup>	81.5	79.9	80.7	1.6
Asp <sup>153</sup> O <sup><math>\delta</math>1</sup> –W–O <sup><math>\epsilon</math>2</sup> Glu <sup>218</sup>	85.2	86.5	85.9	1.3

2

3

4

## Figure legends

**Fig. 1** - Schematic of the expression constructs used for the crystallographic studies. The grey surfaces depict the parts of the proteins expressed and crystallized. Numbers above the bars indicate the amino acid positions. Signal sequences were predicted using the program SignalP [37].

**Fig. 2** - Structural comparison and sequence alignment. **a**, *A. fulgidus* ModA/WtpA (*left panel*) is compared to ModA from *E. coli* (PDB ID 1WOD). The main structural differences are the distorted octahedral coordination of the oxyanion and an additional beta sheet (colored red) in AfModA. **b**, Structure-based alignment of the various ModA/WtpA sequences determined to date. The alignment was performed using DALI-lite [38] followed by minor manual adjustments. Secondary structure motifs are indicated above the sequences, and conserved residues involved in binding of substrate are highlighted in light blue for ModA/WtpA proteins discussed in this study (octahedral coordination) and in light green for ModA proteins with tetrahedral coordination.

**Fig. 3** - Schematic of distinct oxyanion binding sites in related binding proteins ModA/WtpA from *A. fulgidus* (**a**) and ModA from *E. coli* (**b**, adapted from [8]). The schematic highlights the distinct tungsten coordination. Distances are given in angstroms for the two non-crystallographically related AfModA molecules (upper line, chain A; lower line, chain B). For a compilation of the bond angles see Table 2.

**Fig. 4** - Stereo figure of the experimental electron density of the tungstate binding site of AfModA at 1.07 Å resolution, contoured at 3.5  $\sigma$  (blue mesh) and at 60  $\sigma$  (red mesh). For clarity only electron density around amino acid residues directly involved in the binding of  $\text{WO}_4^{2-}$  is

shown. The color code for the atoms is: black=carbon, red=oxygen, blue=nitrogen, yellow=sulfur, green=tungsten. Labels indicate amino acid residues in single letter code.

**Fig. 5** -  $k^3$ -weighted EXAFS spectra (*upper panel*) and corresponding phase-corrected (assuming O in main shell) Fourier transforms (*lower panel*) at the W  $L_3$  edge of tungstate in *A. fulgidus* ModA/WtpA (trace A) and buffer (trace B). Red line, experimental data; black line, simulation with the following parameters (distances in Å, Debye-Waller-type factors as  $2\sigma^2$  in Å<sup>2</sup> in parentheses, Fit Index with  $k^3$ -weighting): trace A, EF -14.619 V, 3 O at 1.786 (0.008), 1 O at 2.060 (0.002), 2 O at 2.241 (0.003), FI  $0.2998 \cdot 10^{-3}$ ; trace B, EF -13.54 V, 3.7 O at 1.770 (0.005), FI  $0.1406 \cdot 10^{-3}$ .



Figures

Fig. 1

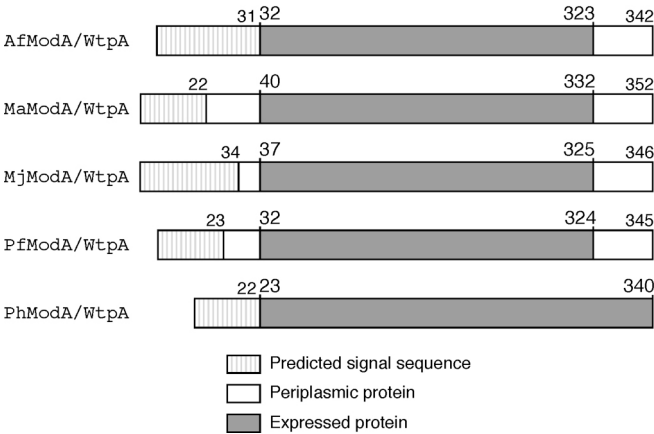
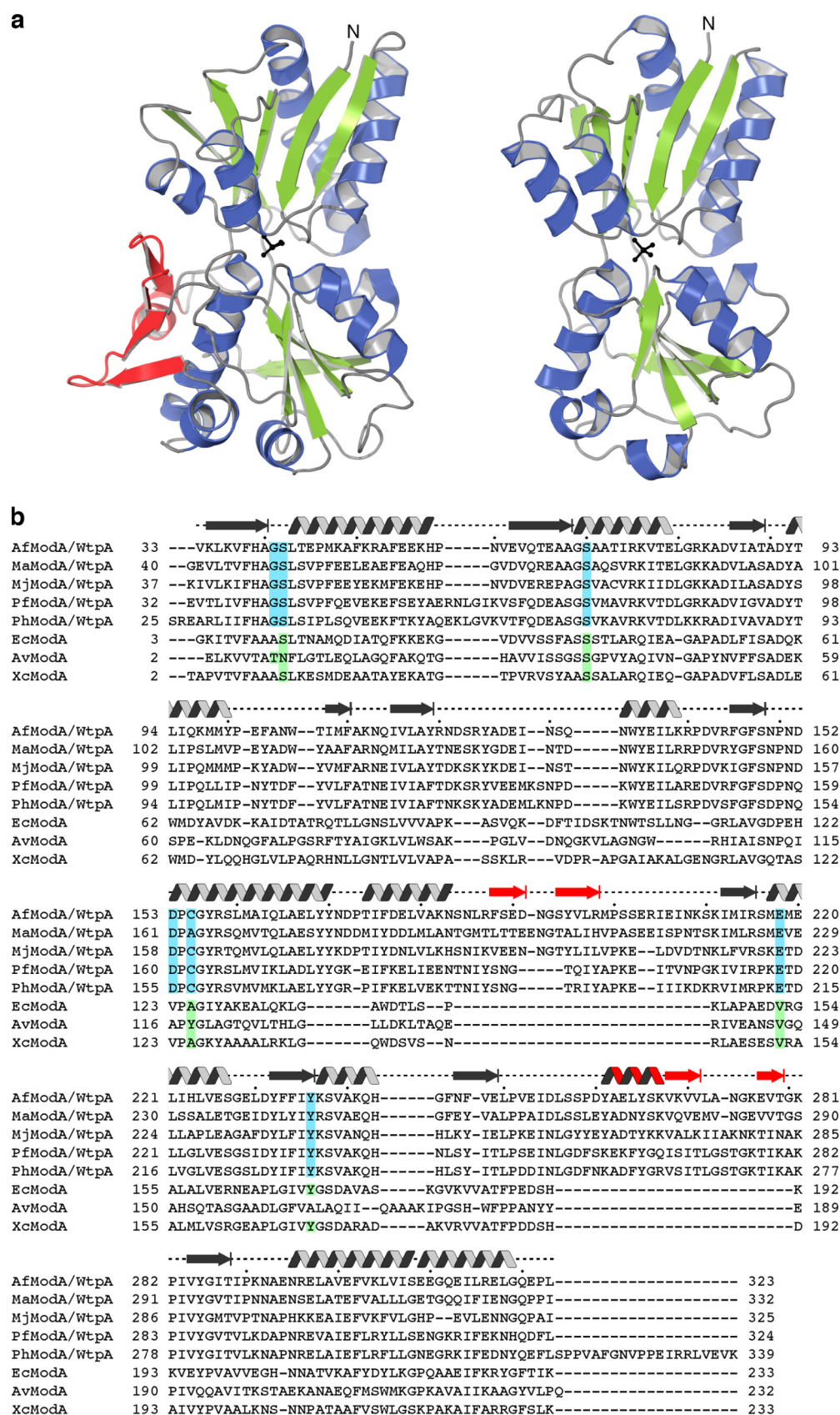


Fig. 2

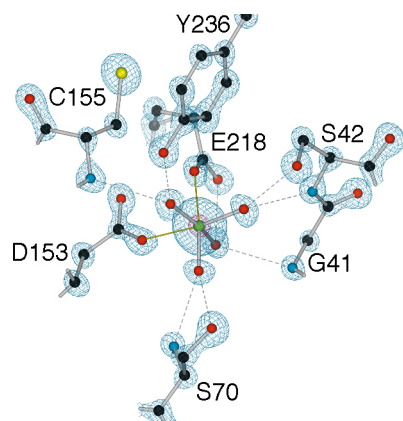


2



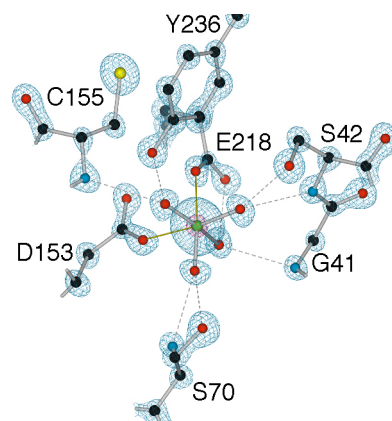
1 Fig. 4

2



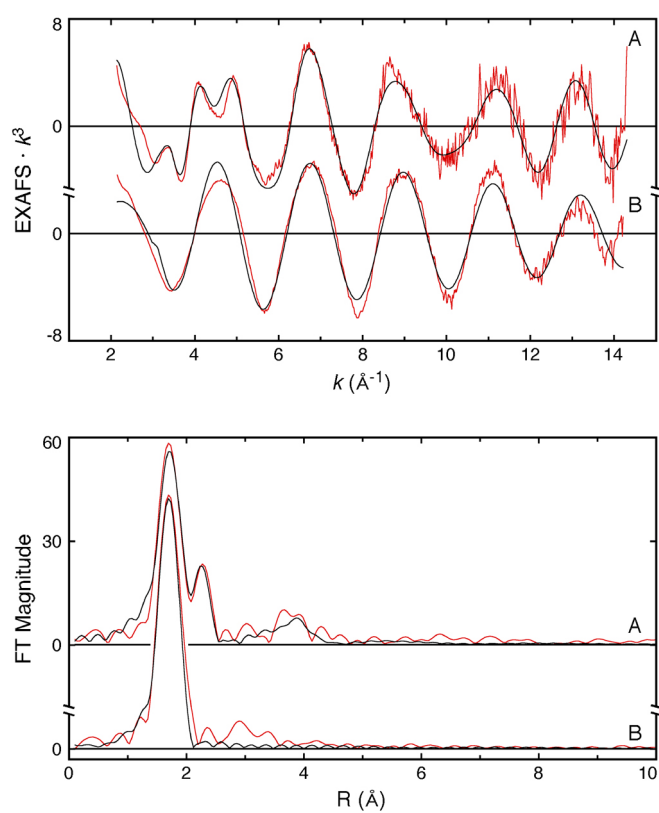
3

4



1 Fig. 5

2



3

4